Ultrasonic velocity survey in Callovo-Oxfordian argillaceous rock during shaft excavation

Cyrille Balland, Jacques Morel, Gilles Armand, Will Pettitt

▶ **To cite this version:**

Cyrille Balland, Jacques Morel, Gilles Armand, Will Pettitt. Ultrasonic velocity survey in Callovo-Oxfordian argillaceous rock during shaft excavation. International Journal of Rock Mechanics and Mining Sciences, 2009, 46 (1), pp.69-79. 10.1016/j.ijrmms.2008.03.011 . ineris-00961932

HAL Id: ineris-00961932

https://hal-ineris.archives-ouvertes.fr/ineris-00961932

Submitted on 20 Mar 2014

HAL is a multi-disciplinary open access archive for the deposit and dissemination of scientific research documents, whether they are published or not. The documents may come from teaching and research institutions in France or abroad, or from public or private research centers.

L'archive ouverte pluridisciplinaire **HAL**, est destinée au dépôt et à la diffusion de documents scientifiques de niveau recherche, publiés ou non, émanant des établissements d'enseignement et de recherche français ou étrangers, des laboratoires publics ou privés.

ULTRASONIC VELOCITY SURVEY IN CALLOVO-OXFORDIAN ARGILLACEOUS ROCK DURING SHAFT EXCAVATION

Cyrille BALLAND[1], Jacques MOREL[2], Gilles ARMAND[2], Will PETTITT[3]

(1) LAEGO-INERIS, École des Mines de Nancy, France, cyrille.balland@ineris.fr

(2) ANDRA, Laboratoire de Recherche Souterrain de Meuse/Haute-Marne, France, jacques.morel@andra.fr, gilles.armand@andra.fr

(3) ASC, Shrewsbury, United Kingdom, will@appliedseismology.com

ABSTRACT

The excavation of a deep underground structure induces a stress field redistribution that could create an Excavation Damaged Zone (EDZ). The study of EDZ is important in the framework of nuclear waste storage, where such EDZ could constitute a preferential pathway of stored material towards the biosphere. Analysis of ultrasonic wave propagation across the rock media around the excavation is one technique that can be used to characterize such zones. This method has been applied in the Meuse/Haute-Marne Underground Research Laboratory (URL) in France to characterise the initialization and evolution of damage around the URL access shaft. To achieve this, a device comprising 21 ultrasonic sensors was spread out at different distances from the shaft wall, at depths of between –465 m and –475 m. A transversal isotropic model enabled the measured experimental velocities on each ray path during shaft excavation to be integrated. The results highlighted the initialization and extension of the damage as the shaft front proceeded. They also showed a polarisation of the velocity field and an oscillation of the transversal isotropy with a preferential orientation of the stress release and the microcracking. Monitoring of the velocity field also highlighted some significantly different behaviour linked to the complex mechanical behaviour of the argillaceous rock.

1. INTRODUCTION

Various studies in the Canadian URL of Lac du Bonnet [1] for granite, Swedish HRL [2] for diorite, Mont Terri [3], Tournemire [4] and Mol [5] for argillaceous rock and Asse [6] for salt rock have shown the presence of a damaged zone around the deep excavations. The characterization of such zones is significant in the safety assessment of nuclear waste underground storage. Such zones could constitute a preferential pathway of radionuclide towards the biosphere. Numerical modelling (mechanical, hydromechanical, etc.) provides a first estimation of the extent and the characteristic of the EDZ. However, the results are strongly dependent on the parameters of the model used and the input data. Consequently, the properties of the traversed rock mass need to be well understood through *in situ* measurements.

Monitoring of ultrasonic wave propagation has demonstrated its capacity to observe the initialization of damage in a previously unperturbed zone. This method is very efficient in granite [7] or in salt rock because wave damping is very low, but it is difficult to apply to argillaceous rock [8]. New technology for optimizing the pulsed energy has been developed in the framework of the European OMNIBUS project [9]. This technology has been directly applied for monitoring the digging of the main shaft of the Meuse/Haute-Marne URL.

The principle of the method is based on the strong dependency of the pressure wave (P-wave) velocity in the rock with the effective stresses and the damage. The objective of this study is to determine the spatial extension of the damage around the shaft and to highlight its evolution as the shaft excavation front progressed. The device has been designed on the basis of the estimation of the extension of the EDZ by numerical modelling and the intensity of the damage with some preliminary laboratory tests on rock samples.

An analysis method was developed to interpret the velocity changes of the ultrasonic waves in a finite volume in terms of orientation and amplitude. The results have enabled the natural heterogeneity and anisotropy of the rock and the nature and the extension of the couple damage/stress variations induced by the shaft excavation to be characterized.

2. EXPERIMENTAL LAYOUT

2.1 SITE AND EXPERIMENT DESCRIPTION

The Meuse/Haute Marne URL is located in the north-eastern part of France, at the boundary between the Meuse and Haute Marne Departments. The research activities carried out by ANDRA (French National Radioactive Waste Management Agency) are dedicated to reversible, deep geologic disposal of high-activity, long-lived radioactive waste [10]. The studied rock formation is a 130 m thick clay formation (argillite) lying at a depth between 420 m and 550 m vertical to the URL. Two 500 m deep shafts give access to the research drifts situated at two levels: a first drift at 445 m depth, accessible from the main shaft, and the main URL level at 490 m depth with several research and technical drifts, accessible from the secondary shaft (Fig. 1).

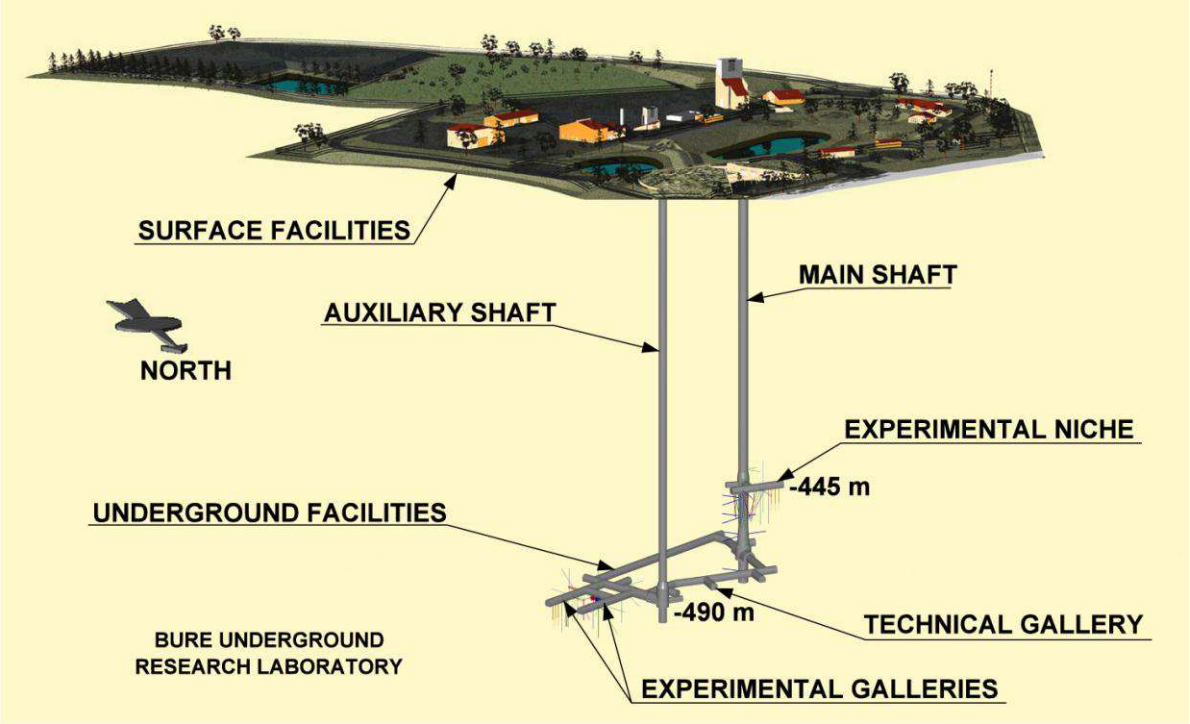

Figure 1: Presentation of the ANDRA URL.

The stress state around the URL has been determined from borehole campaigns from the surface [11]. Principal horizontal stress directions were found to be oriented along N155°E (major stress) and N65°E (minor stress), with a minor stress of about 12.4 MPa and a stress anisotropy of 1.3 at the drift levels. Vertical stress was found to be about 12.7 MPa.

At 445 m depth, the excavation of the main shaft was stopped for the construction of the first drift. From this drift, a specific mine-by experiment, called REP, was carried out. The goal of this experiment was to study the impact of the shaft excavation on the hydromechanical behaviour of the rock mass [12][13]. Several boreholes were drilled from this drift, dipping towards the shaft, and equipped with deformation and pore pressure sensors. The spatial configuration allowed the measurement of the hydromechanical response of the rock mass at different distances from the shat wall and along different orientations. A velocity survey was carried out between 3 parallel boreholes (REP2301 to REP2303) within the REP experiment, to record initialization and evolution of damage around the shaft during and after the excavation phase.

After the instrumentation of the drift, the shaft sinking resumed. The shaft excavation, with a diameter of 6 m has progressed by blasting. The monitoring focused on 10 different blastholes. They are numbered and presented in Fig. 3. The thickness of the removed rock at each blasthole extends from 1.82 to 3.41 m (28 m^3 to 96 m^3) respectively for blasthole 1 and 6. Blasthole 10 (2.76+2.95 m) corresponds to two blastholes, which were reduced to one for the purposes of this study because the acquisition system stopped during this period. For blastholes 2, 6 and 9, the front level was dug deeper with a pneumatic hammer respectively for 40, 70 and 30 cm.

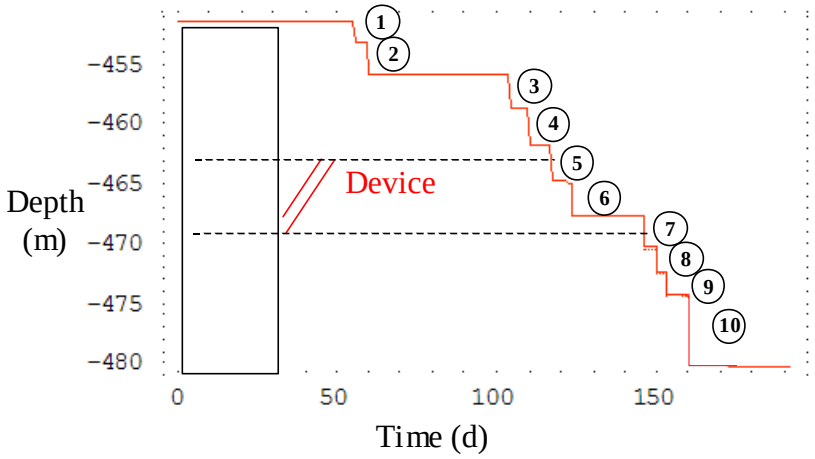

Figure 3: Depth changes of the shaft front during the mine-by test.

2.2 Design and emplacement of the experimental Device

Two key issues have been identified during the design of the velocity device; the way to seal probes with material presenting mechanical properties similar to the claystone and the location of the sensors (distances from the shaft wall, distance between sensors, orientation,…)

Some laboratory tests were performed to choose the best ratio of cement and kaolin mixture following a methodology of material reconstitution and ultrasonic measurement under stress [14]. The cement was chosen for its weak ultrasonic damping. The kaolin was chosen for its low swelling effect (for a clay) and especially its capacity to reduce the compressive strength and the mechanical modulus of the mixture. The objective was to attain the mechanical characteristics of the argillite (Young modulus, Poisson ratio) to avoid a discrepancy between the sealing column and the rock media. The ratio of 15% of kaolin was selected as the best compromise between the modulus and the attenuation.

A constitutive model has been proposed by Andra on the basis of Hoek and Brown criterion [21]. In this generalized Hoek-Brown model, damage in the pre-peak phase is approached by the theory of plasticity and the transition between the brittle failure and the ductile behavior is also integrated as observed from the laboratory characterization on samples. The elastoplastic model uses an associated flow rule with hardening and softening, which exhibits four phases: I-elastic, II-damaged, III-broken, IV-residual. Numerical modelling of the shaft sinking was performed using this model in 3D taking into account the anisotropic in situ stress field and exhibited stresses changes and damaged zones. . On the other hand laboratory tests were performed on samples cored at a depth of –460 m to determine an empirical relationship between mechanical parameters (deviatoric and confining stresses, damaged phase) and the P-wave velocity under different stress path [9][14][16]. This rough empirical law enables the possibility of back calculating, the expected velocity changes around the shaft from the 3D computed stresses in order to determine the location of the probes and sensors.

The experiment device comprises 3 ultrasonic probes 22.41, 22.71 and 23.97 m long (named G1, G2 and G3), installed in 3 parallel and inclined boreholes from the niche at –447 m depth. The target zone of investigation is located near the shaft between the levels –465 m and –475 m. The boreholes were positioned to place the sensors in the zone where the expected velocity changes induced by damage of the rock are the most important. The sensors are located in the last 5 m at the bottom of the probes. The distance between two sensors of the same probe is based on a geometric sequence fitted on the expected velocity change.

The 3 probes comprise 21 ultrasonic sensors and 6 clinometric sensors. The boreholes were drilled end of December 2004, and borehole trajectories were recorded. The velocity survey probes were emplaced using the clinometric sensors to choose the orientation of the ultrasonic sensors along the medians of the device (Fig. 3) . At the end the ultrasonic probes were sealed with the defined mixture of cement and kaolin. The real distance between the ultrasonic sensors and the shaft wall was calculated by linear interpolation between the measured borehole trajectory and the topographic measurement of the shaft wall performed during excavation. This distance ranges from 0.30 to 2.57 m with an accuracy close to 1 cm.

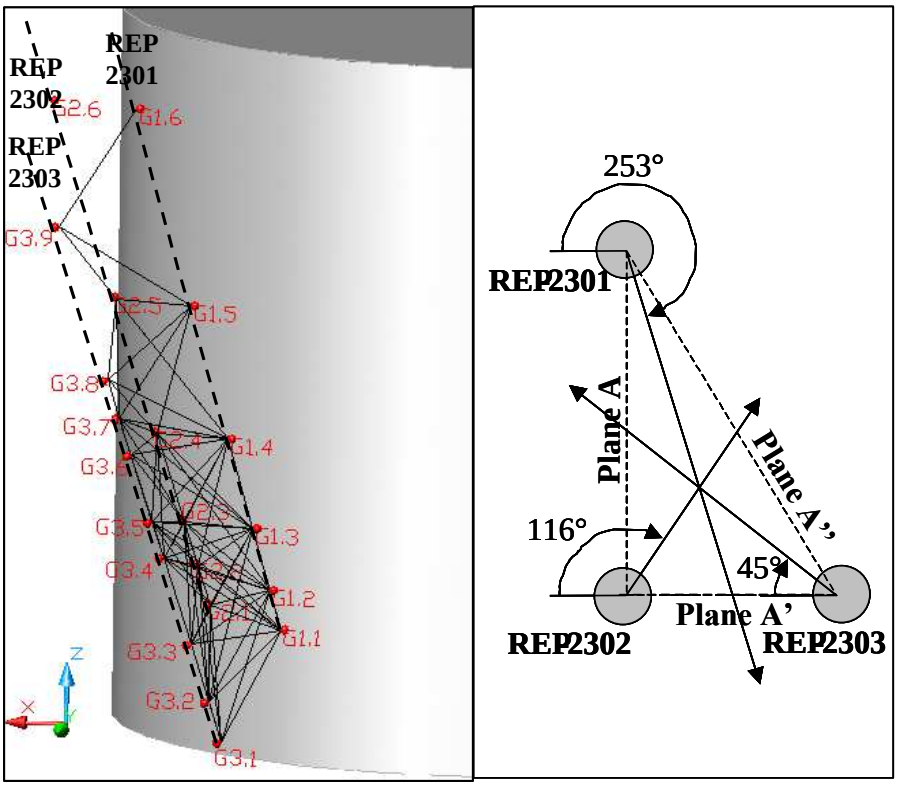

Figure 3: Final experimental device with recorded ray paths and orientation of the probes (view perpendicular to the borehole axis).

2.3 EQUIPMENT

The ultrasonic measurement equipment used in this experiment was developed in the framework of the European OMNIBUS project [9]. One unique feature of this equipment is that it is able to switch automatically the sensors from pulser to receiver using custom-designed pulser-amplifier units. This is in spite of the difference in voltages required for the two modes of operation. During the pulsing it is important to deliver the maximum energy into the rock, and in receiving mode high amplification is required as signals are very low because of the strong damping of the rock media. Therefore, the sensors and associated electronics must be adapted to an alternative voltage of ± 5 V in receiving and 500 V in pulsing.

The OMNIBUS amplifier boosts the ultrasonic signal over a frequency band from 10 to 1000 kHz corresponding to the same frequency band as that of the sensor with a gain from 40 to 60 dB (x100 to x1000). The sensor has been designed to deliver a signal with a frequency peak around 65 kHz corresponding to the optimized frequency for argillaceous media. This frequency is sufficiently high to detect the expected perturbations, but not too high for the energy of the signal to be too damped in a field experiment. The sensors and downhole electronics (pulser-amplifiers) are also designed to withstand the borehole environment, especially regarding resistance to the pore pressures that apply at this depth. They are attached to probes suited to borehole applications. A system with springs provides the coupling of the sensors to the borehole wall while the hooding of the sensors has the same shape as the wall of the borehole.The probes are equipped with systems for injecting sealing material and inclinometric sensors to orientate the body of the probe so that the sensors are in a facing position, so as to maximize the transmitted energy. An interface unit controls the amplifier-sensor pairing. Its first main function is to supply power for the amplifiers and the sensors and to transmit the analogue signals to the acquisition system. Its second main function is to command the running mode of the amplifier-sensor pairing: transmitter or receiver. The other important element of the acquisition unit is the acquisition box that digitizes and transfers the analogue signals to the acquisition computer. 8 GAGE acquisition cards of 2 channels each compose the unit. Each channel samples with a frequency of 10 MHz and a vertical resolution of 16 bits. A computer drives the entire acquisition unit via a software, which controls the continuous monitoring with an automatic acquisition by triggering once a signal threshold is exceeded.

2.4 PROCESSING

The P-wave velocity is the main parameter of this experiment; its absolute value is calculated on the basis of the shortest distance between the transmitters and the receivers and the transit time of the first arrival of the full wave. This velocity does not take account of other bent rays created by velocity gradients in the medium. Consequently, the velocity is measured along a straight ray at the peak frequency of the sensor filtered by the rock (≈65 kHz) and is expressed in metres per second. On the same ray path, unlike the absolute velocity, the velocity change is not much dependant on the exact ray path of the wave. Its calculation is based on the cross correlation of the signals for the same pair of sensors as a function of time. The cross correlation is performed on the first phase of the signal and has an uncertainty of around 1 m/s. However, during shaft excavation, the deformation measurements (measured with extensometers) showed deformations of around 1000 to 2000 μm/m. The distance between two ultrasonic sensors could therefore change by as much during the experiment. This uncertainty is negligible between two closes in time measurements. However, it represents up to a maximum of 6 m/s from the beginning to the end of the experiment.

The absolute uncertainty of the velocity relative to the ultrasonic layout mainly depends on the uncertainty of the positioning of the sensors, which was estimated at ±5 mm. This uncertainty is maximum for the shortest rays (0.7 m). It was estimated at ±17 m/s in this case. This uncertainty applies when the velocities of different rays have to be compared, but not when one compares velocity variations.

The estimation of the transversal anisotropy of the medium in terms of velocity is based on the hypothesis of a punctual approximation of the device. In other words, velocity variations from one ray to the next only depend on the anisotropy, which is considered as homogeneous over the entire volume. The anisotropy probably changes from one point to another, especially according to the lithology and the deconfinement/damage pairing. However, the number of rays and their spatial distribution are too low, to provide sufficient spatial resolution, so just one anisotropic value is calculated for the entire device. The anisotropy estimation method is based on the non-linear fit of the experimental data following the form function defined by Thomsen [17]:

$$V(\theta) = V_m + A\cos^2(\theta - \theta_m)\sin^2(\theta - \theta_m) + B\sin^4(\theta - \theta_m) \qquad (1)$$

where:

V P-wave velocity (m/s);

V_m maximum velocity (m/s);

θ incidence angle of the ray compared to the horizontal (rad);

θ_m phase angle difference where the velocity is maximum;

A and B coefficients respectively represent the slope and the amplitude of the anisotropic model.

Since the velocity is, in principle, little dependent on the azimuth of the rays, it is possible to assume transversal anisotropy. The anisotropic calculation can therefore be extended to the third dimension on the basis of a symmetrical revolution around the direction of the main minimum velocity, which, in this case, is close to the vertical direction. We sought to generalise the incidence angle of the rays over the whole horizon by assuming:

$$(\theta - \theta_m)^2 = (x - x_m)^2 + (y - y_m)^2 \quad (2)$$

where x and y are the coordinates of the ray in the stereographic presentation respectively in the east and north direction.

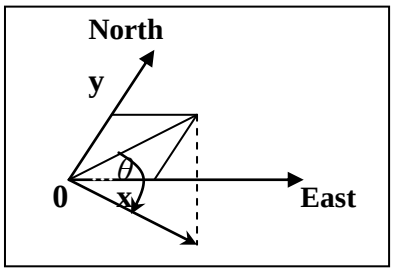

with *(1)* and *(2)*:

$$V(x,y) = V_m + A\cos^2\left[\sqrt{(x-x_m)^2+(y-y_m)^2}\,\sin^2\left[\sqrt{(x-x_m)^2+(y-y_m)^2}\right]^2\right] + B\cos^4\left[\sqrt{(x-x_m)^2+(y-y_m)^2}\right] \quad (3)$$

The estimation of the transversal anisotropy is calculated with a Levenberg-Marquart type resolution [18][19]. The transversal isotropy model is applied to each series of velocity field measurements, which makes it possible to determine several indicators that take all the data into account. These indicators are determined from the parameters of equation (3). They are defined by the extremes and the phase differences of the equation representing respectively the maximum and minimum amplitude, the azimuth and the dip of the main velocities. The anisotropy model integrates all the ultrasonic rays and extracts the strong trends corresponding to the perturbation affecting the sounded rock volume. The results can be represented graphically by the regression surface that minimizes the discrepancy with the experimental data.

3. RESULTS

The results presented in this paper correspond to the raw data of 461 measurement runs with 15 to 18 emissions each. That represents about 17,000 different signals over the whole acquisition period from the 13th January to the 25th July 2005. The total number of transmitted ultrasonic rays was theoretically 272 per run with the final configuration. However, taking into account the distribution of the device over 5 m and the damping of the rock, the total number of rays that could be recorded and interpreted at the start of the acquisition was 115. The maximum distance covered by the ultrasonic wave in the argilites was 1.95 m, consistent with the 2 m maximum observed in the EZ-A and ED-B experiment of the Mont Terri URL [8][20].

The signal to noise ratio of the recorded signals depends on the orientation and the length of the rays. The noise level was around 70 mV high and the maximal amplitude of the strongest signals experienced distortion and reached 1 V. So the signal to noise ratio varied from 0 dB to 22 dB respectively for 1.95 and 0.76 m ray lengths. The signals were processed in this study for a signal to noise ratio over 5.

3.1 NATURAL VELOCITY CHANGES

In the ultrasonic device, some rays constitute 3 by 3 triangles located along the same sub horizontal planes at different depths. The rays between G1 and G2 are very close to parallel to the shaft wall (plane A), the rays between G2 and G3 are close to the perpendicular (plane A') and the rays between G1 and G3 are close to the oblique line (≈45°, plane A''). The first measurements of the P-wave velocities on these rays showed an important change of the original velocity according to depth (fig; 4). For example, the velocity varied from around 300 m/s from –465.15 to –466.19 m (1.05 m) for the sensors G2.2-G3.4 and G2.4-G3.6 respectively. This vertical variability is in accordance with the natural gamma radioactivity, but does not satisfy the hypothesis of homogeneity used for the estimation of the initial anisotropy. This hypothesis of a homogeneous field may introduce a bias in the initial anisotropy estimation. However, this bias is avoided for the analyse of the anisotropy change during the shaft excavation using a differential analysis.

The fitting of the velocity data, according to the ray angle incidence and the previously defined anisotropic model, showed an initial transversal isotropy up to 14.2 % with a phase difference of 17.4° to the East and 3.1° to the North. Therefore, the isotropy is not exactly transversal but presents a slight orientation in the horizontal plane (lithology plane) mainly to the east. This deviation may come from the initial stress field anisotropy. This initial orientation and its consequences are always taken into account in the modelling of anisotropy.

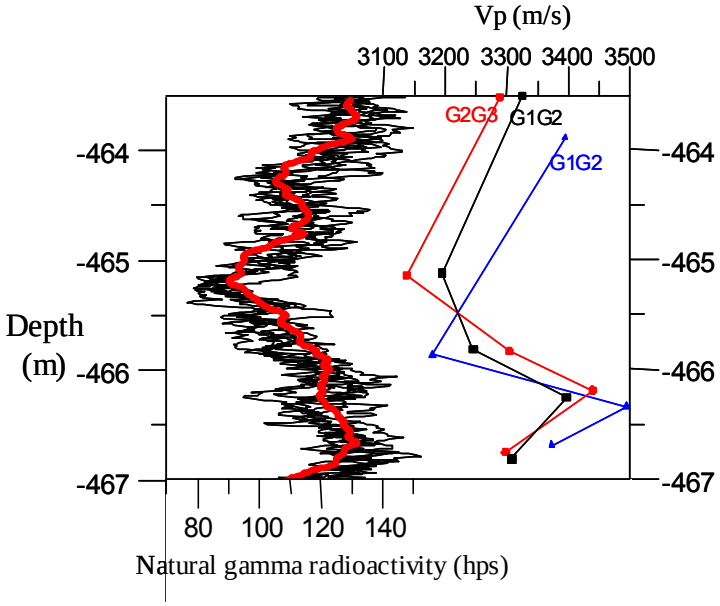

Figure 4: P-wave velocity changes for horizontal rays in comparison with natural gamma radioactivity (data provided by ANDRA and recorded by SEMM).

3.2 TEMPORAL VELOCITY CHANGES

Fig. 5 shows the global velocity changes on few representative rays between two ultrasonic probes compared to the shaft front level. The P-wave velocity is approximately constant before the excavation of the shaft reaches a level 8 m above the ultrasonic network. A significant velocity decrease occurs as the shaft advance reaches the level of the instrumented network, the magnitude of the velocity decrease measured on the ray paths depending on sensors location. Velocity continues decreasing, moderately and gradually, as the excavation of the shaft progresses deeper.

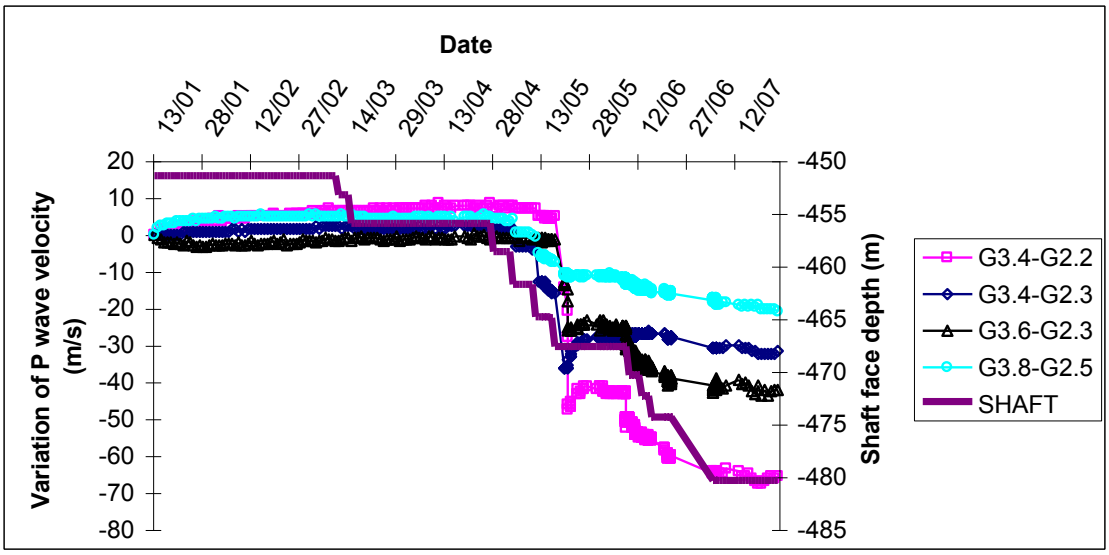

Figure 5: Temporal velocity changes on few representative ray path during the mine-by-test.

Since the ultrasonic sensors closest to the shaft wall are located between –469.7 and –468.7 m deep, it is therefore logical that the blasthole 6 (between –464.9 and –467.6 m on the 17/05/05 further extended to –468.3 m on the 20/05/05) created the biggest disturbance.

The example of Fig. 6 shows the evolution on 4 typical rays of the impact of the 6th blasthole. This blasthole caused an acquisition cut where the velocity data are missing. The impact of this blasthole can be broken down into two stages: (1) from A to B, a drastic and generalized decrease of the velocity just after the blasthole and (2) from B to C, an increase for the majority of the rays; only the rays the farthest from the shaft wall continued to decrease or stabilize.

The velocity of the ray G3.8-G2.5 decreases slightly after the 6th blasthole and stabilizes from the 21/05/05. The velocity of the other rays decreases first, reaches a minimum before starting increasing. The ray G3.4-G2.3 reacts quicker than the others, reaching its minimum velocity value before the 20/05/05 at 4pm, while the two others rays G3.6-G2.3 and G3.4-G2.2 reach it only on the 21/05/05 at 12am. Consequently, the increase in the velocity does not start at the same time for each ray.

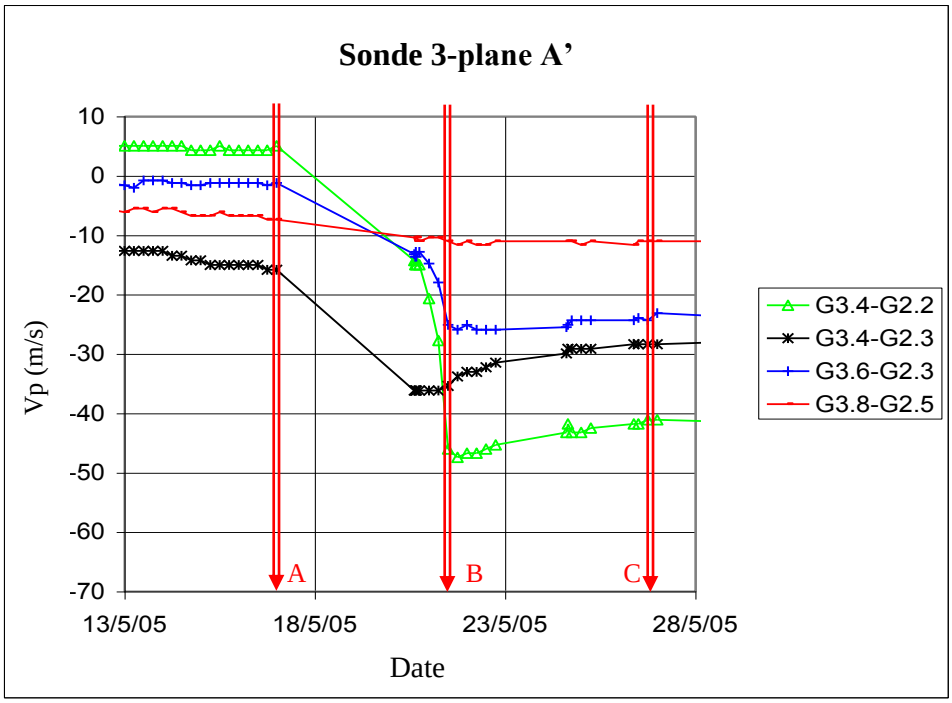

Figure 6: Effects on velocity during the 6th blasthole.

Fig. 7 presents the stereonets (i.e. velocity changes as a function of ray orientation) of the velocity for different stages of the shaft excavation. The first variations affect the rays with a dip very close to the vertical (shaft front at a depth of –455.9 m and –461.7 m), then at –464.9 m the velocity changes along an axis close to that of the minor horizontal stress (N65°E). This means the rays close to the plane passing through the vertical and with the azimuth N75°E are the most affected. After the most disruptive blasthole between 464.9 and –467.6 m, all the rays are affected by a velocity decrease with a bipolar tendency.

The least disrupted rays were oriented along an axis with an azimuth between N90°E and N130°E and between N270°E et N300°E with, in this same zone, a minimum disruption of rays with the lowest dip;

The most disrupted rays were oriented along the complementary azimuths N60°E and N240°E corresponding to the direction of the minor horizontal stress after the boring of the shaft. These two angular zones of major change tended to extend over subsequent blastholes. The affected rays were the ones with a dip less than 50° and azimuths between N310°E and N80°E and between N130°E and N260°E.

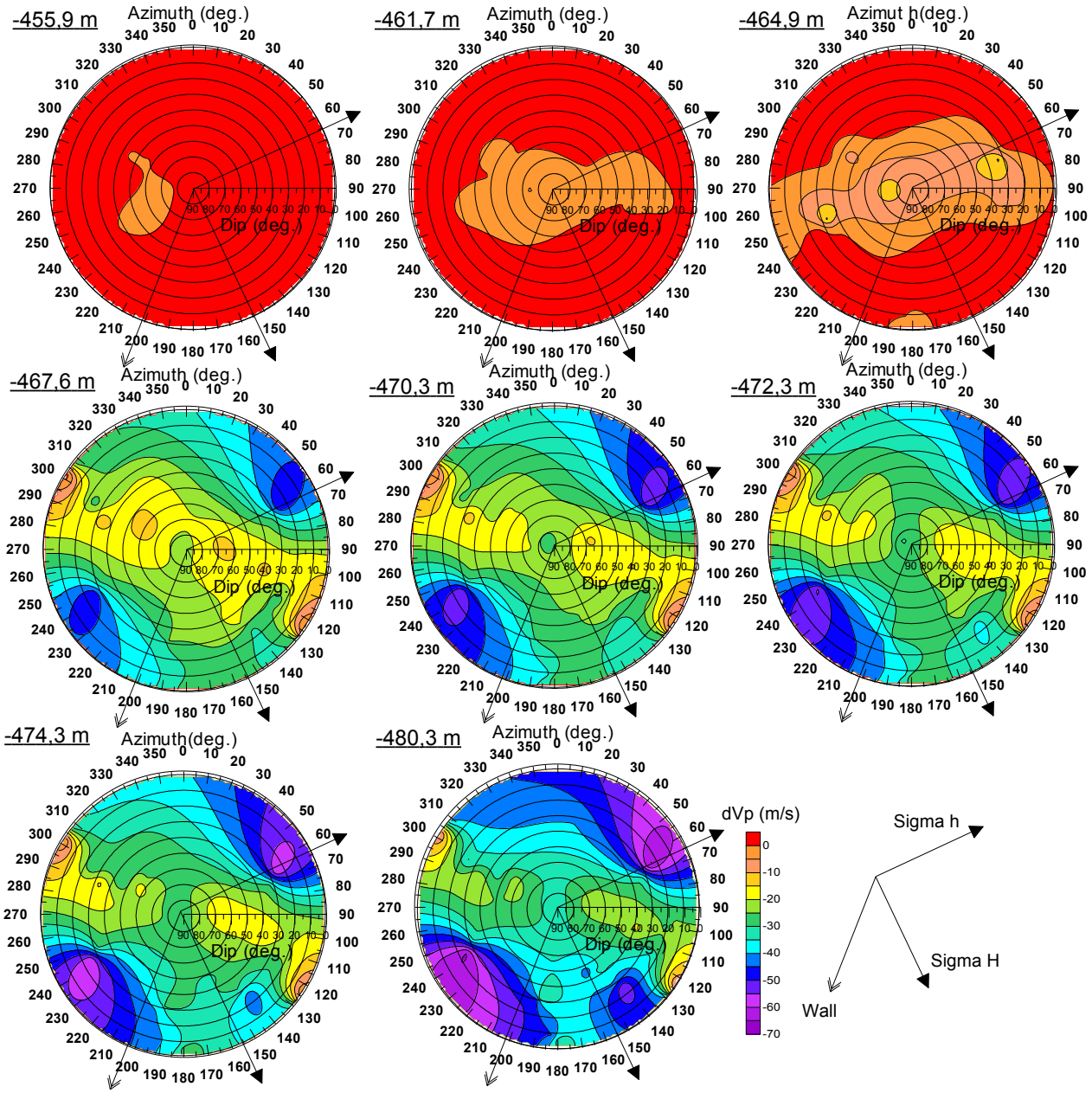

Figure 7: Stereonets of the velocity changes at different stages of the shaft excavation.

A focused analysis of the velocity changes just after the 6th blasthole (Fig. 8) shows that the disturbance is mainly for subhorizontal rays in the direction of the horizontal minor stress, what confirms the general trend of the experiment. The rays in the direction of the major horizontal stress show only a very slight decrease in velocity. The results also show an alignment of the rays most affected by a velocity increase along the N70°E-N250°E direction. At the same time, the rays, in the direction perpendicular to this axis show a slight velocity decrease.

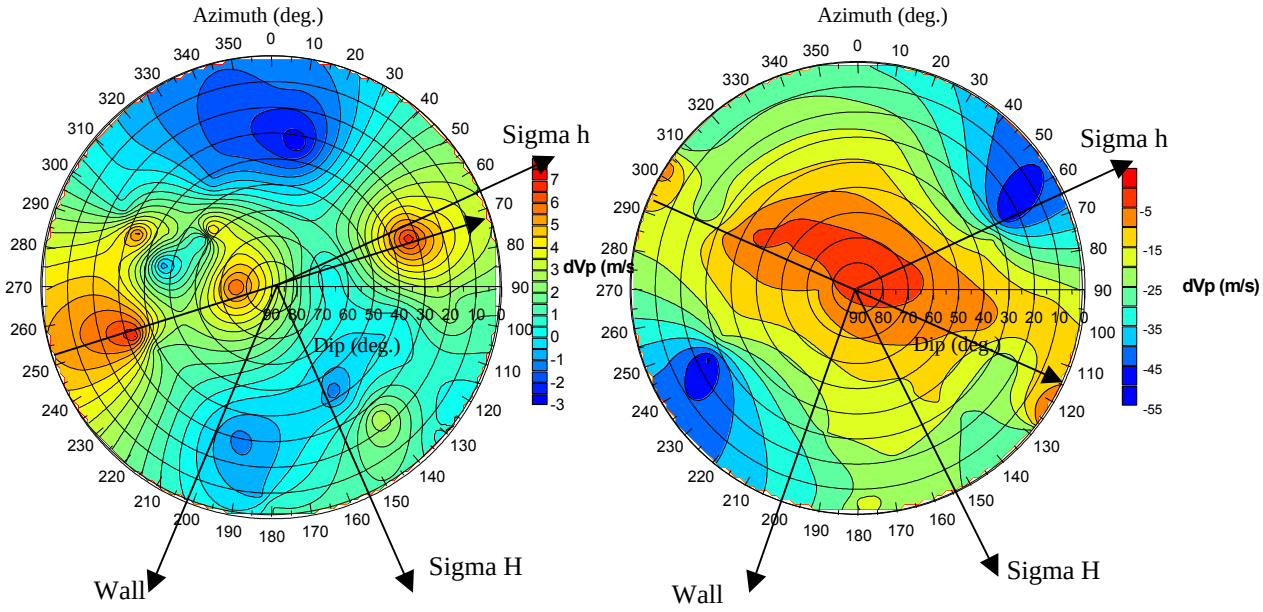

Figure 8: Stereonets of the P-wave velocity just after the 6th blasthole on the right (B-A) and for the velocity rebound on the left (C-B).

3.3 SPATIAL VELOCITY CHANGES

For each ray, the velocity changes are presented according to their distance from the shaft wall (Fig. 9). The distance corresponds to the barycentre of the transmitter-receiver pairing. This spatial presentation has been broken down into three significant steps of the experiment: (1) the initial state corresponds to the average of the velocity for each ray obtained with ten measurements just after a weak velocity increase during the first days of the experiment (shaft front at a depth of –451 m); (2) the intermediate state corresponds to an average obtained for each ray over ten measurement points immediately after the blasthole 6 (shaft front at a depth of –468 m); and (3) the final state based on an average, for each ray, of the last ten measurements of the acquisition (front at a depth of –480 m).

The velocity changes during the experiment were overall largest close to the shaft wall and decreased with increasing distance. Two main zones could be distinguished. A first zone close to the shaft wall, with a majority of rays that showed a velocity change over 30 m/s. This zone extends to a distance of 1.6 m from the shaft wall. The maximum variation was attained at 0.7 m from the shaft wall with -67 m/s. There is a second zone where the velocity varied less than 20 m/s over 1.6 m.

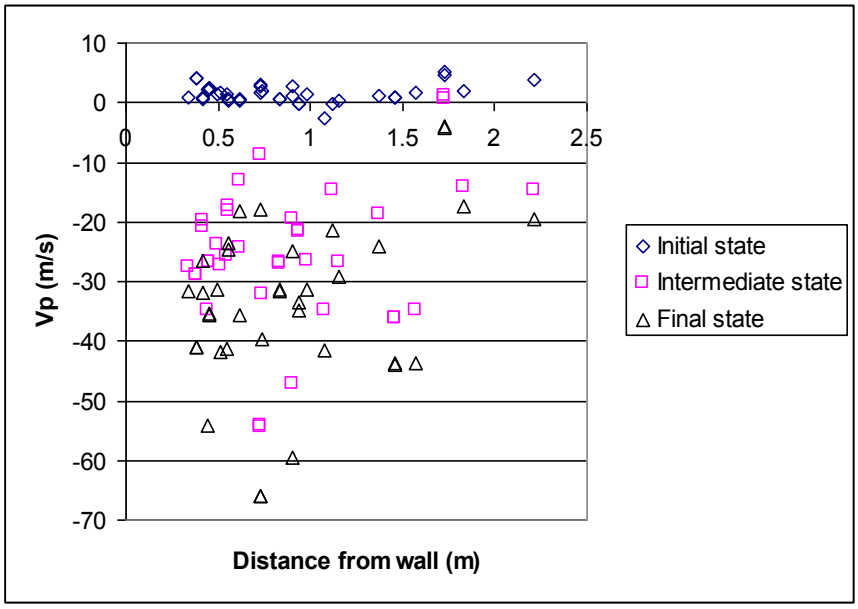

Figure 9: P-wave velocity change according to shaft wall distance for the initial, intermediate and final states.

The increase in velocity measured on some rays just after the 6th blasthole seems to affect only the sensors in the first metre of rock (zone 1) although the blasthole 6 disturbed rock through 1.6 m (zones 1 and 2 in Fig. 10).

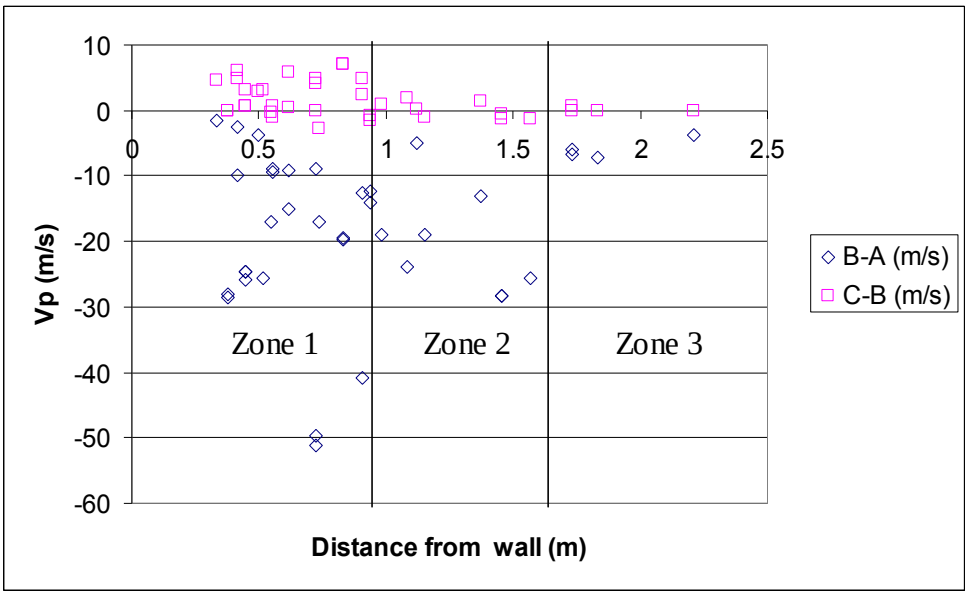

Figure 10: Velocity changes as a function of the distance from the shaft wall during the 6th blasthole.

3.4 ANISOTROPIC MODEL

The extended transversal anisotropic model explained previously enabled an integration of all the raw data. The model provided the overall evolution of the velocity throughout the analysed rock volume. The results are presented on the curves of the variations of the model parameters as a function of time and shaft front progress.

The curves of the main velocities (minimum and maximum velocities, Fig. 11 and Fig. 12) clearly have a stepped shape with (1) a stable period with initial velocities close to the ones of the unperturbed rock, (2) a drastic decrease during the shaft crossing for the maximum velocity direction and more moderate for the minimum velocity direction and (3) a period with a slight velocity decrease after the shaft has gone past.

The decrease in the velocity is significant but remains moderate, around 40 m/s in the direction of the maximum velocity (lithology plane) and around 30 m/s along the vertical. Therefore, the perturbation of the shaft excavation seems to be more limited along the vertical axis. In addition, the velocity decrease in the lithology plane is mainly concentrated during the period just after the blasthole 6, while the decrease along the vertical is distributed over all the blastholes. The minimum velocity is close to the vertical and is influenced earlier as the shaft front and the associated unloading comes, whereas the maximum velocity, close to the horizontal, is influenced only as the shaft front is going past.

The velocity increase at the beginning of the experiment shows two different flow rates that can be seen on the maximum velocity curve (Fig. 16-a). The first flow rate corresponds to the first days after the installation of the probes with a moderate but rapid increase in the velocity of several metres per second. The amplitude of the second flow rate is similar to the first but the velocity change is slow and spread out over the 100 first days of the experiment.

The evolution of the anisotropic factor (ratio between the minimum and maximum velocities) shows the combined effect of the disturbance of the strongest velocities and the weakest velocities. Fig. 16-c shows a greater sensitivity than the ones provided by the changes in the two main velocities analysed separately, particularly for the minimum velocity. From the first blastholes, the anisotropic factor tends to increase by 0.1%. Nevertheless, the biggest changes occur between the blastholes 3 and 9. During the blastholes 3, 4 and 5, the anisotropic factor increases by 0.3 %, decreases by 1 % during the blasthole 6 and finally increases during the blasthole 7. After this last blasthole, the anisotropic factor decreases to a plateau value of 0.3 % below the initial anisotropic factor.

The main anisotropic directions show some weak but significant changes that drive a rotation to the north. This rotation is more significant in the main direction of the high velocities. The oscillation already observed on the anisotropic factor is also highlighted for its orientation, especially with the dip for the direction of the highest velocity. More precisely, the dip increases while the azimuth decreases before the arrival of the shaft front at the level of the device. When the shaft front goes past the device, then the tendency is reversed to levels higher than the initial state.

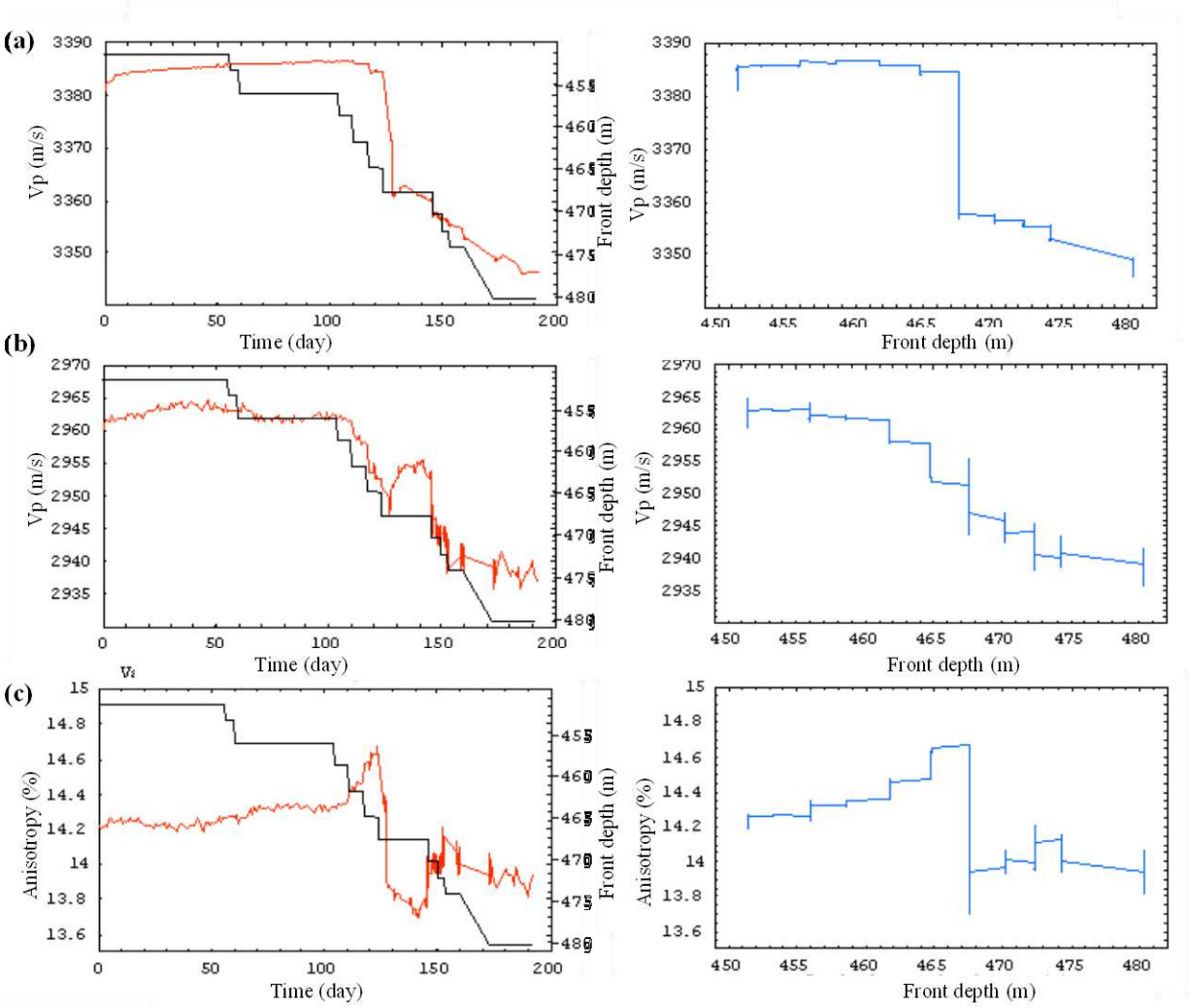

Fig. 11: **(a)** P-wave change of the maximum velocity versus time (on the left) and shaft depth (on the right). **(b)** P-wave change of the minimum velocity versus time (on the left) and shaft depth (on the right) **(c)** Anisotropic factor change versus time (on the left) and shaft depth (on the right).

The relationship between velocity change and shaft position forecasted by numerical modelling 1 m from the shaft wall is similar to the average of the velocity change of the anisotropic model (average of the velocity in all directions). This is highlighted by an initial decrease 10 m behind the shaft front and a typical step after the shaft has gone past. However, the amplitudes of the variations diverge by a factor of 10 (Fig. 12) and are discussed further below.

The small amplitude of velocity variations measured with the velocity survey device is consistent with the measurements performed in the shaft just after the excavation. Indeed, as the shaft front was at a depth of 468.3 m, the excavation was stopped more than 2 weeks to allow different kinds of measurements to be done. Seismic refraction performed on the shaft wall and seismic profiles carried out in a radial borehole showed that velocity variations did not extend deeper than a few tenth of centimetres; the resolution of these methods was lower (the frequency was about ten times lower), but it confirms that velocity variations are very small in the volume investigated by the velocity survey.

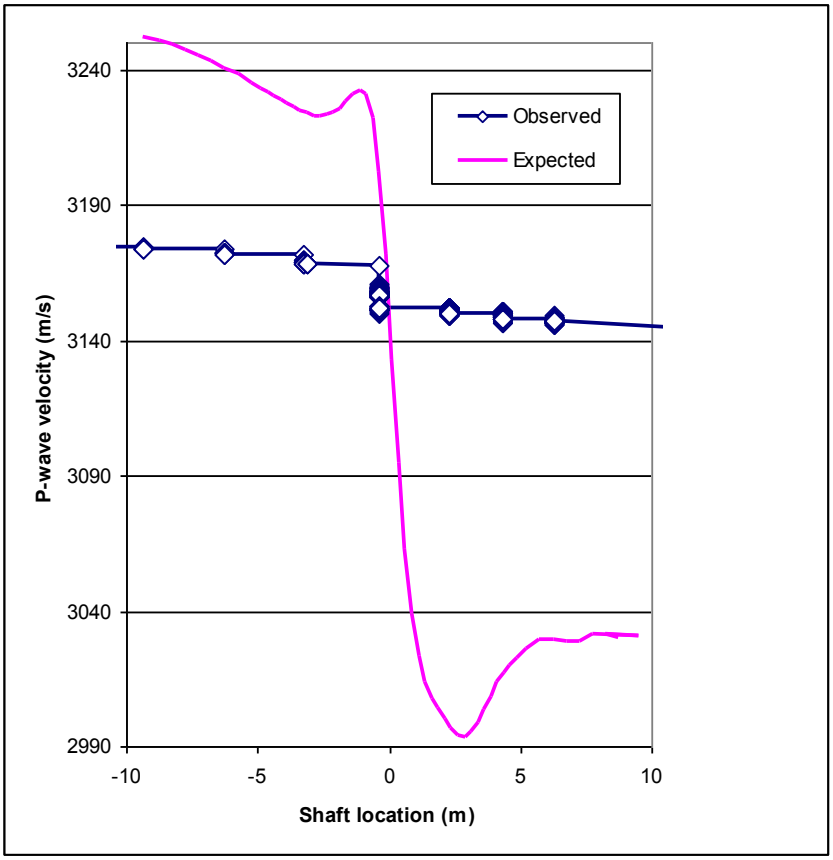

Fig. 12: Comparison between the expected velocity change at 1 m from the shaft wall and the average velocity change observed on the device as a function of the shaft front progress.

4. DISCUSSION

4.1 NATURAL VARIABILITY OF THE VELOCITY

The natural variability of the P-wave velocity in argilites is 12% depending on the depth and 14% depending on the dip of the rays. The natural rock is therefore both heterogenic and anisotropic. This variability is greatly superior to the one induced by the shaft excavation. It is only 2% at the maximum.

The velocity variability as a function of depth also affects the estimation of the velocity variability as a function of the orientation of the rays. The extension of the network needs to be sufficient to have a good angular cover of the rays and so this extension necessarily covers a rock volume characterized by a certain heterogeneity. However, in this experiment, the spatial distribution of the rays was sufficiently random for the angular variability to clearly stand out despite the fact that the angular variability is of the same order of magnitude as the spatial variability. It is this natural variability that is expressed in the form of a mainly transversal anisotropy. It comes from the sedimentary structure of argilites with the series of the lithologic interfaces and the preferential orientation of the mineral layers [22]. The waves propagate quicker along the interfaces and along the mineral layers than when propagating perpendicular.

The average anisotropy estimated by the ultrasonic device between -463 and -469.7 m deep is 14.2%. This is higher than the anisotropy estimated on samples by laboratory tests (10%) at a depth of –460 m in the same facies. This difference can be linked: (1) to the scale difference between the sample and the *in situ* rock volume, which is caused by a network of lithological interfaces of size greater than the test sample (70x140 mm), (2) homogeneous damage following the deconfinement and desaturation during the sampling, which decreases the anisotropy by the same amount.

4.2 DYNAMIC OF THE VELOCITY CHANGES

Therefore, only 2% of the velocity changes are linked to the deconfinement and the damage to the argilites. The drilling of the boreholes itself probably created a disturbance of the velocity field. This disturbance tends to reach equilibrium through reconfinement within the first few days of the experiment (corresponding to the observed measurement increase) due to the slightly expansive properties of the cement-kaolin mixture and a slow resaturation in the immediate borehole vicinity. The disturbances only caused by shaft excavation (Fig.13) are mainly characterised by: (1) the initiation of the velocity decrease from the blastholes situated 10 m from the instrumental device; it is greater and earlier on the subvertical rays (in the shaft axis); (2) a maximum of disturbance during the shaft crossing with the higher amplitudes on the rays perpendicular to the shaft wall and for the rays located in the zone between 0 to 1.6 m from the wall; (3) a velocity increase just after the drastic decrease (velocity rebound) around the shaft front up to 1.6 m behind the front and up to 1 m from the wall, especially for the rays oriented in the direction of the minor horizontal stress; and (4) a weak oscillation of the amplitude (1%) and the dip (0.4°) of the anisotropy during the shaft crossing and finally a rotation of the velocity field to the north.

These measurements seem to indicate initially a deconfinement of the rock ahead of the front and logically oriented along the vertical stress. It is subsequently followed by a stronger deconfinement and perhaps slight damage with microcracking parallel to the shaft wall. This damage, probably complex due to the heterogeneities of the rock, the irregularities of the shaft wall surface and the corresponding stress field, is nevertheless progressive and inversely proportional to the distance from the shaft wall. It seems to be contained within the first 1.6 m of the rock. Other evidences confirm that damage zone is small, with a low level decreasing with depth. For example, permeability measurements performed in the vincinity of the shaft [12] show that the most significant permeability increases (one order of magnitude) are detected in the zone very close to shaft wall up to 1 m, small increases (less than one order of magnitude) remains measurable up to 2 m and to 2.5 m depending the orientation to the stress field. Displacement measurement indicates that displacement in the direction of the major horizontal stress is nearly elastic and extent of plastic zone remains small [12]. Numerical analysis (cf. chapter 2.2 and [25]) exhibits 1.5 m of damaged zone in the direction of minor horizontal stress. All those data are coherent with the velocity field described herein.

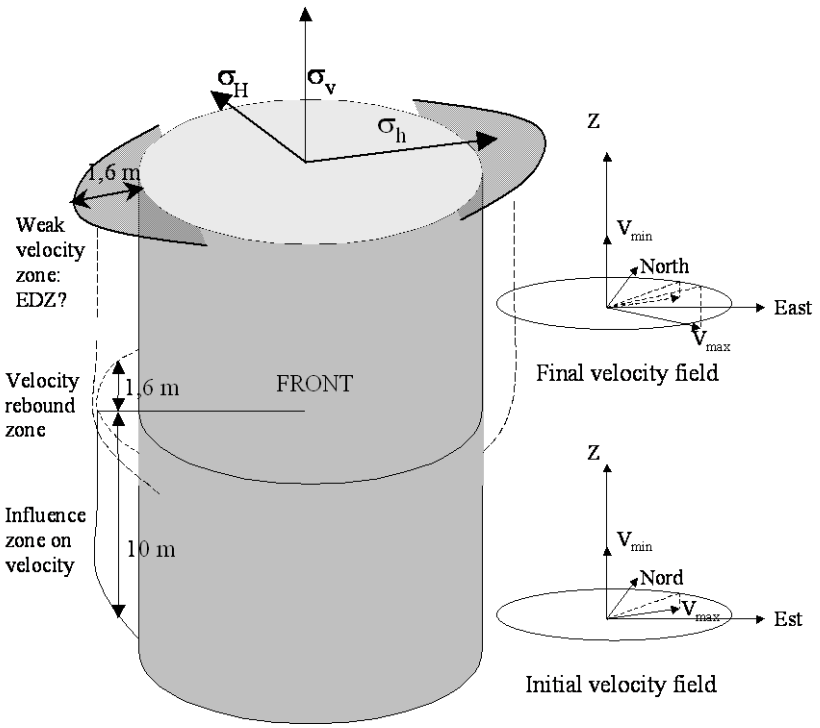

Fig. 13: Interpretative figure of the velocity changes during the mine-by test.

The oscillation of the anisotropic factor during the mine-by test can be linked in part to pure elastic phenomena such as reorganization of the stress field and in part to irreversible phenomena such as rock damage in the vicinity of the shaft (induced anisotropy). Laboratory tests on Callovo-Oxfordian argilites [9] have shown that the initialization of an anisotropic decrease corresponds to the damage initialization. In fact, the anisotropy in this rock is induced mainly by the asymmetric nature of its layered structure. Inducing a random microcracking tends to reduce the difference between the velocity along the layers and across the same layers. This phenomenon is further intensified by the preferential orientation of the deconfinement perpendicular to the shaft wall and the lithology.

The reorientation of the velocity field is due to the rotation of the stress field during the shaft crossing. The minor horizontal stress σ_h tends to rotate towards the shaft axis, in which the radial stress on the wall surface is zero (assuming the argilites are not very plastic). At the same time, the major horizontal stress σ_H tends to rotate towards an axis orthoradial to the shaft with a maximum close to the surface. The velocity changes depend on the value of the ratio of the applied stress divided by the tensile strength of the rock [23] and the direction of propagation of the studied waves. In fact, depending on the level of the applied stress, either the existing cracks will close (low stress), or new cracks will be created (high stress). In the case of weak stress, it is the cracks perpendicular to said stress that will close preferentially. In the case of high stress, cracks parallel to said stress are created, which induces a decrease in the velocity of the waves that propagate perpendicularly to the stress direction [24].

The rock is clearly deconfined along the radial axis of the shaft and the deviatoric stress could create some microcracking parallel to the shaft wall. However, it is very difficult to determine the contribution of each phenomenon on the wave velocity decrease. The laboratory tests and the numerical modelling used to forecast the velocity changes have overestimated their amplitude by an order of magnitude. This difference can stem from the stress field modelling, especially as regards the uncertainty of the input parameters used at that time (modulus level, stress anisotropy, etc.). The difference also can stem from the laboratory tests, which are not sufficiently relevant to represent damage phenomena on a large scale. Triaxial tests that exactly reconstitute the same stress path in the sounded rock volume would doubtless be more representative. In addition, the duration of the tests could be the determining factor of this difference. The laboratory tests were performed over several hours, whereas the mine-by test lasted several weeks. Different phenomena such as the viscous behaviour of argilites could reduce the initialization or the opening of the cracks. Whatever the case, the velocity changes are slight and consequently the damage generated by the shaft is low.

Furthermore, the instrumental device is at the same time too big to sound a layer of homogeneous argilites and too small to sound the whole rock medium around the shaft. The results of this experiment focused on a limited area next to the shaft, so it is not yet possible to know if the extent and the level of the perturbation vary around the entire shaft and, in particular, if the perturbation is lower on the side of the direction of the major horizontal stress.

4.3 VELOCITY REBOUND

A non-negligible transitory phenomenon seems to be associated with the irreversible damage and stress release phenomena in the immediate vicinity of the front (1 m). This is reflected by an increase in velocity and seems to propagate with, for example, an increase of 7 m/s for example for the ray G3.4-G2.2. This phenomenon is clearly highlighted by the change of the velocity anisotropy. However, this phenomenon is difficult to understand at the state of our present knowledge and simply on the basis of the ultrasonic velocity. However, we can put forward three hypotheses. This increase could be due to: (1) changes in pore pressure; in fact in the direction of the horizontal minor stress instaneous over pressure are observed due to hydromechanical coupling under an anisotropic state of stress with a low permeable media [12]. Over pressure are observed before the front reaches the level of the sensor and when the front crosses the level of a sensor, high peak of pressure appears followed by a pressure drop down. (2) The displacement of the stress front ahead of the shaft front during the progress of the shaft by punctual attack with pneumatic hammer; however the punctual attack with a pneumatic hammer only concerns the last meter of the velocity survey device, while the rebound is observed on rays at the level or even above the shaft front. (3) Blast effect which induces stress redistribution around the measurement boreholes which can affect the measurements. After, the creep behaviour could explain the increase of velocity.

As the next excavation steps resume it is difficult to say if the rebond is just a way to reach equilibrium or if it is linked with a transitory phenomemum. Further information and analysis are required to better explain it.

5. CONCLUSIONS

The excavation of the main shaft in the argilites of the Meuse/Haute-Marne URL significantly disrupted the velocity field. Monitoring of the P-wave anisotropy during the mine-by test enabled the singular behaviour of the ultrasonic rays to be eliminated while retaining information from each one.

The velocity field deteriorated from 10 m ahead of the shaft front with a maximum disruption during the shaft crossing. This disturbance decreased progressively up to 1.6 m from the shaft wall. The shaft crossing creates an oscillation of the main velocity directions with a significant velocity drop initially and then a differed velocity rebound. Finally, the order of magnitude of the velocity changes showed that deconfinement and damage to the rock were limited. It confirms that the level of damage is low and that the EDZ extent remains small. Those results are coherent with other measurements performed in the vicinity of the shaft (permeability and deformation measurements and other seismic methods) and with elastoplastic 3D modelling (even if measured velocity field is not in accordance in term of amplitude with the one back calculated from the 3D modelling results with an empirical relationship).

The experimental device is very sensitive but cannot clearly separate the deconfinement and damage contribution in the disruption and only sounded a limited area around the shaft. The measurement of the damping of the waves, the transmission of a full shear wave signal and the integration of an orthotropic component in the anisotropic model would improve understanding of the microcracking and the rock damage phenomena.

References

[1] Martin CD, Read RS and Martino JB. Observations of brittle failure around a circular test tunnel. Int J Rock Mech Min Sci 1997; 34: 1065–1073.

[2] Pettitt WS., Baker C, Young RP, Dahlstrom L, and Ramqvist G. The assessment of Damage Around Critical Engineering Structures Using Induced Seismicity and Ultrasonic Techniques. Pure and Appli Geophysics 2002; 159: 179-195.

[3] Thury M and Bossart P. The Mont Terri rock laboratory, a new international research project in a Mesozoic shale formation. Switzerland Eng Geol. 1999; 52 :347–359.

[4] Bonin B, Deep geological disposal in argillaceous formations: Studies at the Tournemire test site. J Contam Hydrol. 1998; 35: 315–330.

[5] Mertens J, Bastiaens W and Dehandschutter B. Characterization of induced discontinuities in the Boom Clay around the underground excavations (URF, Mol, Belgium). Appli Clay Sci 2004; 26: 413–428.

[6] Hou Z. Mechanical behaviour of salt in the excavation disturbed zone around underground facilities. Int J Rock Mech Min Sci 2003; 40: 725–738.

[7] Carlson SR and Young RP. Acoustic emission and ultrasonic velocity study of excavation-induced microcrack damage at the Underground Research Laboratory. Int J Rock Mech Min Sci 1993; 30: 901–907.

[8] Forney F. Caractérisation par méthodes ultrasoniques de la zone endommagée induite par le creusement d'un tunnel en milieu argileux : Cas d'étude au tunnel du Mont Terri, INPL Thesis, 1999.

[9] Pettitt WS, Young RP, Balland C, Collins DS, Hildyard MW, Bigarré P and Lebon P., Development of the Tools and Interpretation Techniques for Ultrasonic Surveys to Monitor the Rock Barrier around Radioactive Waste Packages in Geological Repositories, OMNIBUS Final Technical Report, FIKW-2001-00202, Fifth EURATOM Framework Program EC, 2004.

[10] Delay J, Vinsot A, Krieger JM, Rebours H, Armand G. Making of underground scientific experimental programme at the Meuse/Haute-Marne underground research laboratory. North Eastern France, Phys Chem of the Earth 2007, 32: 2-18.

[11] Wileveau Y, Cornet FH, Desroches J and Blümling P. Complete in situ stress determination in an argillite sedimentary formation. Phys Chem of the Earth 2007; 32: 866-878.

[12] Armand G and Su K. Hydromechanical coupling phenomena observed during a shaft sinking experiment in a deep argillaceous rock, Proc Geoproc Nanjing, May 2006, p. 725-731.

[13] Souley M, Su K, Armand G and Ghoreychi M, Poromechanical behaviour of deep claystone and permeability changes around shaft. Int. Workshop on Constitutive Modelling - Development, Implementation, Evaluation, and Application, 2007, Hong Kong, China.

[14] Darot M, Reuschlé T. Acoustic wave velocity and permeability, evolution during pressure cycles on a thermally cracked granite, Int. J. Rock Mech Min Sci 2000; 37: 1019-1026.

[15] Bieniawski ZT. Mechanism of brittle fracture of rock. Part II – experimental studies. Inter J Rock Mech Min. Sci 1967; 4: 395-406.

[16] Paterson M. Experimental Rock Deformation - The brittle field, Springer-Verlag, Berlin Heidelberg New York, 1978.

[17] Thomsen F, Weak elastic anisotropy. Geophysics 1986; 51: 1954-1966.

[18] Levenberg K. A Method for the Solution of Certain Problems in Least Squares. Quart Appl Math 1944; 2: 164-168.

[19] Marquardt D. An Algorithm for Least-Squares Estimation of Nonlinear Parameters. J. Appl Math 1963; 11 : 431-441.

[20] Damaj J. Auscultation et surveillance des perturbations hydromécaniques d'ouvrages souterrains par méthodes ultrasonores. INPL Thesis, 2006.

[21] Souley M, Su K, Ghoreychi M and Armand G. Constitutive models for rock mass: numerical implementation, verification and validation in FLAC and Numerical Modeling in Geomechanics. Lisse, ISBN 2003; 90 5809 581 9: 71-80

[22] Référentiel géologique du site de Meuse/Haute-Marne, Tome 4 : Le callovo-oxfordien. Rapport ARP ADS99-005, 2001.

[23] Lockner D, Walsh JB and Byerlee J. Changes in seismic velocity and attenuation during deformation of granite, J Geophys Res 1977; 82: 5374–5378.

[24] Nur A and Simmons G. Stress-induced velocity anisotropy in rocks: an experimental study. J Geophys Res 1969; 74: 6667–6674.

[25] Souley M., Armand G., Su K., Wileveau Y. Modelling of the hydromechanical response of a shaft sinking in a deep claystone, tenth International Symposium on Numerical Models in Geomachanics NUMOG X, 25-27 April 2007, Rhode, Greece : 269-275